Article

Journal of the Brazilian Chemical Society

https://dx.doi.org/10.21577/0103-5053.20240083

J. Braz. Chem. Soc. **2025**, *36*, 1, e-20240083, 1-11

Poly(amidoamine) Dendrimer Modified with Terminal Hydroxyl Functional Group as an Efficient Alternative for CO_2 Capture

Thiago M. Rossi,*[*,a] Monique L. Almeida,[b] Mariana M. V. M. Souza,[c] Elizabete F. Lucas[a,d] and Bluma G. Soares[a,d]

[a]*Programa de Engenharia Metalúrgica e de Materiais/COPPE/LADPOL, Universidade Federal do Rio de Janeiro, Av. Horácio Macedo, 2030, Bloco F, 21941-598 Rio de Janeiro-RJ, Brazil*

[b]*Programa de Engenharia Química/COPPE, Universidade Federal do Rio de Janeiro, Av. Horácio Macedo, 2030, Bloco G, 21941-972 Rio de Janeiro-RJ, Brazil*

[c]*Centro de Tecnologia, Escola de Química, Universidade Federal do Rio de Janeiro, Bloco E, Sala 206, 21941-909 Rio de Janeiro-RJ, Brazil*

[d]*Instituto de Macromoléculas/LMCP, Universidade Federal do Rio de Janeiro, Av. Horácio Macedo, 2030, Bloco J, 21941-598 Rio de Janeiro-RJ, Brazil*

Poly(amidoamine)-type dendrimers (PAMAM) were synthesized by divergent routes, and generations (G0.5, G1.0, G1.5, G2.0 and G2.5) along with hydroxylated half-generation polymers (G0.5-OH, G1.5-OH and G2.5-OH) were characterized by Fourier-transform infrared spectroscopy, thermogravimetric analysis and differential scanning calorimetry. Carbon dioxide (CO_2) capture tests were performed using thermogravimetric analysis. Among the absorption temperatures tested, 60 °C was the most promising: 0.77, 1.08, and 1.14 mol CO_2 L^{-1} for G0.5-OH, G1.5-OH and G2.5-OH, respectively, of CO_2 and partial pressure of 45 kPa. This showed that dendrimers with larger molecular structures have more hydroxyl groups and consequently capture more CO_2. However, at low partial pressures (< 2 kPa), CO_2 solubility in PAMAM increased with temperature reduction, confirmed by Henry's solubility constant (398.4 mol m^{-3} kPa^{-1}, in G2.5-OH at 40 °C). According to the thermodynamic properties of CO_2 solubilization, the process was spontaneous ($\Delta G_{sol} < 0$) and exothermic ($\Delta H_{sol} < 0$).

Keywords: absorption, carbon dioxide, PAMAM, dendrimer

Introduction

Human activities are mainly responsible for consuming natural resources. Greenhouse gas emissions and the resulting global warming are stimulating governmental policies for environmental preservation and expanding the scientific discussion to many sectors of society.

According to the National Oceanic and Atmospheric Administration (NOAA), in 2021 the concentration of carbon dioxide (CO_2) in the atmosphere was 414.72 ppm, a record even with the economic crisis caused by the coronavirus disease (COVID-19) pandemic.[1] This was the fifth highest annual growth of CO_2 emissions (2.58 ppm). The International Energy Agency (IEA) highlighted that in 2020 the global health crisis caused a 6% reduction in CO_2 emissions from burning fossil fuels, showing the importance of having greater control over the main global energy sources.[2] In addition, Brazil emitted 2.09 billion tons of CO_2 in 2015 and 2.28 billion tons in 2016, placing the country as the seventh largest polluter in the world.[3]

Studies from the IEA have predicted a growing tendency for CO_2 emissions, reaching 42.9 billion tons by 2030 due to deforestation, cement production, and use of non-renewable energy sources such as natural gas, oil, and coal. However, the IEA also has reported that in 2021 there was recovery of CO_2 emissions from combustion, reaching the highest level since the beginning of measurements, 36.3 gigatons (Gt), a 6% increase in relation to 2020.[4] The Intergovernmental Panel on Climate Change (IPCC) 2022 pointed out that

*e-mail: marconcinirossi@hotmail.com
Editor handled this article: Fernando C. Giacomelli (Associate)

from the pre-industrial era to date, 2.4 trillion tons of CO_2 have been emitted to the atmosphere, 58% from 1850 to 1989 and 42% from 1990 to 2019. In addition, 17% of all carbon emitted to date has been released into the atmosphere over the last 10 years, indicating the urgent need to reduce greenhouse gas release.[5]

There are three main approaches to CO_2 separation and capture: solid adsorption, liquid absorption, and membrane purification. However, these techniques have operational limitations in terms of pressure, temperature and materials. Commonly, gases from burning are emitted at high temperatures, requiring cooling to capture CO_2, making the process more expensive.[6] Zeolites have been widely used as solid adsorbents for CO_2 capture. They are porous materials containing metal ions that occur naturally in nature or can be synthesized in the laboratory. However, these materials require high energy consumption in the regeneration process.[7] Absorption in liquids is a well-established technology, normally using amine solutions that can react with CO_2 to capturing it. Despite this, some drawbacks exist, such as high energy consumption for regeneration, carbon steel corrosion and easy degradation.[8,9] The CO_2 separation using membranes integrated with ionic liquids is a promising technique, since it has high selectivity and efficiency. On the other hand, the membranes operate at high pressure, which requires high energy consumption, and are expensive to synthesize.[7]

Dendrimers are macromolecules with a branched three-dimensional structure and many functional groups on their surface. Poly(amidoamine) (PAMAM) is the most common dendrimer type. It is structured by bonded monomers to form ramifications from a core.[10]

The outer layer of PAMAM dendrimer can have amines or hydroxyls as the basic functional groups, which present excellent properties for capture of acid gases like carbon dioxide, making them potentially useful to capture greenhouse gases. Using dendrimers to capture CO_2 is a technological innovation to reduce the carbon footprint, since few studies have been published in the last 20 years.

Most studies have used membranes to separate CO_2 from gas streams. However, the CO_2 separation operation presents problems when the process is fed with low CO_2 partial pressures, since the gas flow is not high enough to achieve good performance. The operational range of CO_2 partial pressure of systems using membranes varies between 100-600 kPa (high pressure).[11-17] In other methods, the dendrimer is grafted onto solid inorganic materials and CO_2 capture is performed in an adsorption process.[18,19] Fadhel *et al.*[18] reported that the ability to adsorb CO_2 on SBA-15 silica was improved when amine-terminated dendrimers were impregnated into the porous inorganic structure. Furthermore, the authors showed that the pure dendrimer had low capacity to capture CO_2. Shah *et al.*[19] carried out a study using organoclays, where an amine-terminated dendrimer was loaded into laponite, hydrotalcite and sericite clays, with the organoclays of laponite having the best CO_2 adsorption capacity.

However, these studies were performed with PAMAM-type dendrimers containing an amine-terminal functional group. Furthermore, the processes used were separation by membranes and adsorption on porous materials. In this article, we propose CO_2 in a liquid phase absorption process using dendrimers containing terminal hydroxyl functional group and operating at atmospheric pressure. This is a system where the corrosive effect of these dendrimers is less than those containing an amine functional group. In addition, the operation at atmospheric pressure has lower energy cost.

Therefore, this article evaluates the CO_2 absorption capacity of three different PAMAM dendrimer generations containing hydroxyl basic terminal groups (G0.5-OH, G1.5-OH, and G2.5-OH), by varying absorption temperature and CO_2 partial pressure. The PAMAM generations were produced by divergent synthesis and then analyzed using Fourier-transform infrared (FTIR) spectroscopy, thermogravimetric analysis (TGA), and differential scanning calorimetry (DSC).

Experimental

Materials

The reagents and solvents used in the synthesis of dendrimers were supplied from Sigma-Aldrich (Barueri, Brazil).

The equipment used for data acquisition was purchased from Thermo Fisher Scientific (Waltham, USA) for infrared spectroscopy and from TA Instruments (New Castle, USA) for thermal analysis and absorption tests.

PAMAM dendrimer synthesis

The poly(amidoamine) synthesis method was based on Tomalia *et al.*[20] and Froimowicz *et al.*[21] The chemical structures of the molecules were built from an ethylenediamine (EDA) nucleus by divergent synthesis.

The synthesis procedure of the PAMAMs was similar to that performed by Barros *et al.*[22] For PAMAM generation 0.5 (G0.5) synthesis, 9 mL of EDA, 53 mL of methyl acrylate (MA), and 80 mL of methanol were added to a 250 mL two-neck round-bottom flask fitted with a N_2 gas inlet and outlet to ensure a moisture-free atmosphere. A

Michael addition reaction was processed under magnetic stirring at 500 rpm for four days at room temperature. Other dendrimer generations were synthesized using the same experimental conditions. After each reaction step, the products obtained were distilled under vacuum at 60 °C.

PAMAM generation 1.0 (G1.0) was synthesized through amidation reaction for 11 days by mixing 33 g of G0.5 with 24 mL of EDA in an alcoholic medium. Generation 1.5 (G1.5) was synthesized by reacting 23 g of G1.0 with 35 mL of methyl acrylate for four days using methanol as solvent. Generation 2.0 (G2.0) was synthesized by reacting 33 g of G1.5 with 16 mL of EDA for 21 days in alcoholic solution, and generation 2.5 (G2.5) was synthesized through a Michael addition reaction for four days by mixing 19 g of G2 and 21 mL of acrylate in alcoholic medium.

The terminal functional groups of generations G0.5, G1.5, and G2.5 were modified to incorporate basic hydroxyls. For these reactions, a 250 mL two-neck round-bottom flask was also used, fitted with N_2 gas inlet and outlet, at room temperature, and 500 rpm magnetic stirring. At the end of each reaction step the products were vacuum distilled at 60 °C.

PAMAM G0.5-OH was produced by reacting 3 g of G0.5 with 3 mL of diethanolamine (DEA) in 40 mL of ethanol for 27 days. G1.5-OH was produced by reacting 3 g of G1.5 with 3 mL of DEA for 45 days in an ethanol solution, and G2.5-OH was produced reacting 3 g of G2.5 with 3 mL of DEA for 54 days. The structures were synthesized and evaluated for CO_2 absorbance as shown in Figure 1.

PAMAM dendrimer characterization

The functional groups of the synthesized dendrimers were identified by infrared spectroscopy in the wavelength range from 4000 to 400 cm^{-1} using a Nicolet ISO50 FTIR with attenuated total reflectance (ATR) accessory. The TGA analysis was carried out in a TA Instruments Q50 analyzer, containing about 7 mg of sample under nitrogen atmosphere (100 mL min^{-1}), heated from 25 to 600 °C at a 10 °C min^{-1}. The DSC analysis was performed in a TA Instruments Q500, with a 7 mg sample under nitrogen atmosphere, cooled to –90 °C in the first cycle and heated to 90 °C in the second cycle, both at a rate of 10 °C min^{-1}.

CO_2 absorption capacity tests

Absorption capacity tests were carried out in a TA Instruments SDT Q600 thermogravimetric analyzer in a CO_2/N_2 stream with different CO_2 mole fractions (Table 1). Stream flow was kept at 100 mL min^{-1}. PAMAM samples of approximately 28 mg were heated to 90 °C at 20 °C min^{-1}, and then the temperature was maintained for 1 h to perform *in situ* sample drying. Afterward, samples were cooled at 20 °C min^{-1} to their respective target absorption temperatures (40, 60, 80 or 90 °C) and the CO_2 stream was released for 2 h. The partial pressure of CO_2 (p_{CO_2}) was calculated using equation 1, where p_{atm} is the atmospheric pressure (101,325 kPa) and x_{CO_2} is CO_2 molar composition.

$$p_{CO_2} = p_{atm}\, x_{CO_2} \quad (1)$$

CO_2 solubility thermodynamics

Gas-liquid absorption is related to gas-phase solubility in liquids. In ideal solutions, solutes and solvents obey Raoult's law.[24] However, in low-concentration (dilute) real solutions, solute molar concentration in liquid-phase ($[CO_2]$) is proportional to solute partial pressure in gas-phase (p_{CO_2}), and the proportionality constant (K_H) is called Henry's solubility constant (Henry's law, equation 2).[24]

It is important to highlight that the CO_2 partial pressure ideal curve is tangential to its experimental one only at low CO_2 concentrations where the solution is diluted enough to be considered ideal.[24] The K_H value (in mol m^{-3} kPa^{-1}), which indicates the CO_2 in PAMAM solubility, can be calculated at relative low pressures as the slope from linear fitting of experimental data.[25]

$$[CO_2] = K_H p_{CO_2} \quad (2)$$

From Henry's solubility constant, which correlates CO_2 amount in gaseous and liquid phases, it is possible to estimate the enthalpy of the solution (ΔH_{sol} in kJ mol^{-1}), Gibbs' energy (ΔG_{sol} in kJ mol^{-1}) and entropy (ΔS_{sol} in kJ mol^{-1} K^{-1}). The ΔH_{sol} is related to interaction forces between the liquid and the dissolved gas,[26,27] ΔG_{sol} to chemical process spontaneity, and ΔS_{sol} to the system degrees of freedom.[24] Equations 3 (Van't Hoff equation) and 4 describe these thermodynamic relationships.

Table 1. CO_2 mole fractions and partial pressures of gas mixtures

x_{CO_2}	0.45	0.35	0.25	0.15	0.05	0.02	0.01	0.007
p_{CO_2} / kPa	45.60	35.46	25.33	15.20	5.07	2.03	1.01	0.71

x_{CO_2}: CO_2 molar composition; p_{CO_2}: partial pressure of CO_2.

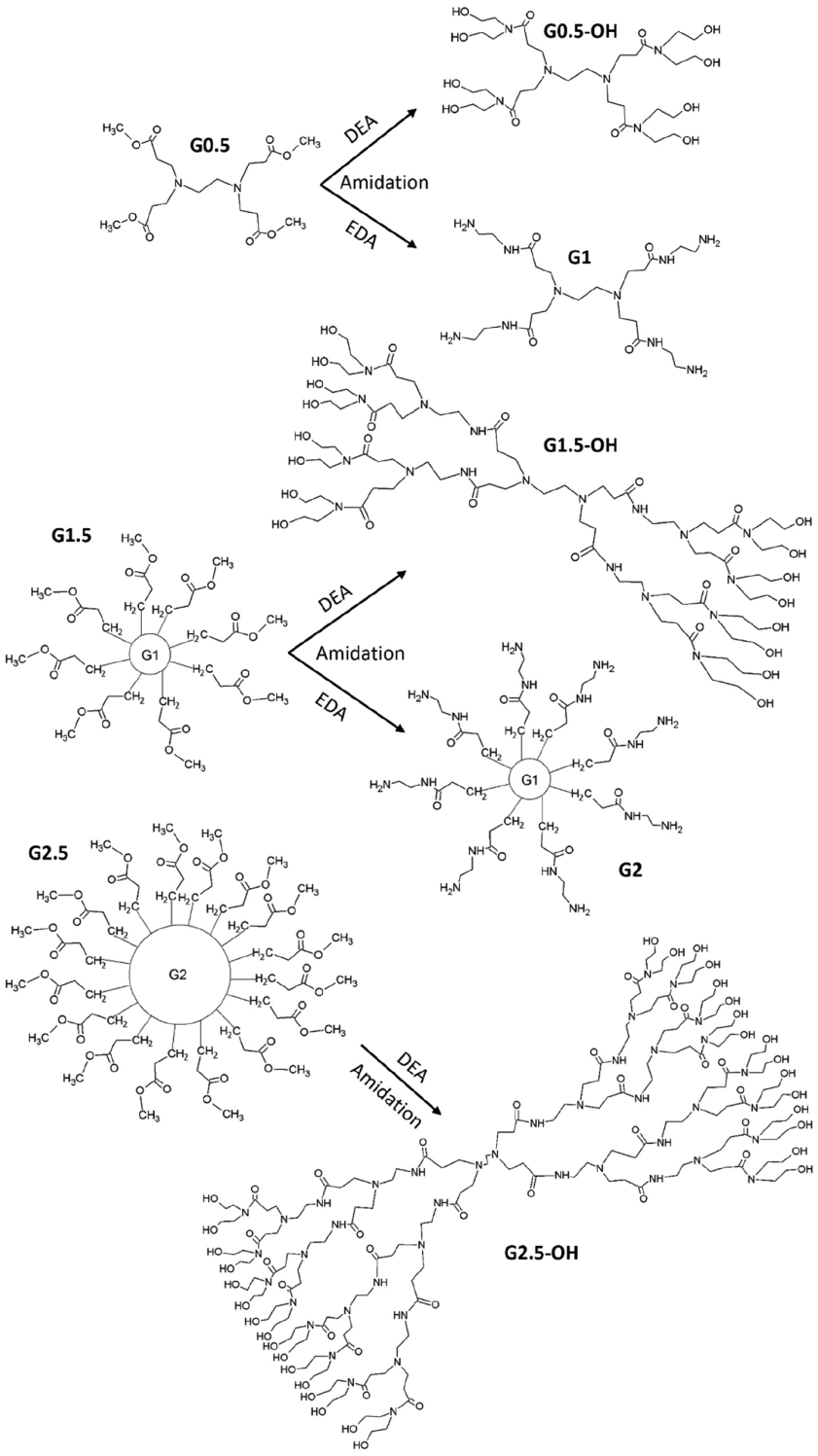

Figure 1. Structures of PAMAM dendrimer synthesized in this work (adapted from reference 23).

$$\ln\left(\frac{K_H}{K^*}\right) = \frac{-\Delta H_{sol}}{R}\frac{1}{T} + \frac{\Delta S_{sol}}{R} \quad (3)$$

$$\Delta G_{sol} = -RT\ln\left(\frac{K_H}{K^*}\right) \quad (4)$$

where K^* is the Henry solubility constant of CO_2 in water at 298 K (0.34 mol m^{-3} kPa^{-1}, reference), R is the ideal gas constant (J mol^{-1} K^{-1}), and T is the temperature in Kelvin (K). ΔH_{sol} and ΔS_{sol} were calculated by the linear fit from a 1/T *vs.* $\ln(K_H/K^*)$ graph.

Results and Discussion

Dendrimer characterization

Figure 2 shows the infrared spectra of the synthesized dendrimers: G0.5, G1, G1.5, G2, and G2.5. The molecules were successfully synthesized, since the spectroscopic profiles resembled those reported by Kannaiyan and Imae,[28] Niu *et al.*,[29] Şenel and Çevik,[30] Şenel *et al.*,[31] and Cao *et al.*[32] More characterization details can be found in our previous work.[23]

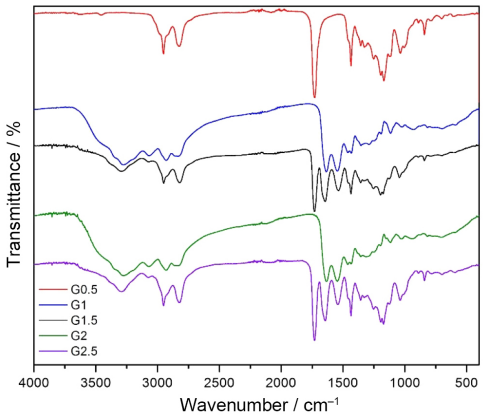

Figure 2. Infrared spectra of PAMAMs with ester end group (G0.5, G1.5, and G2.5) and amine end group (G1 and G2).

Figure 3 depicts the infrared spectra of dendrimers with hydroxyl groups in the outer layer. As expected, the free hydroxyl band at 3295 cm^{-1} is wide and intense. Likewise, a high-intensity C–O stretching band for primary alcohols at 1044 cm^{-1} confirms the existence of a polyalcohol chain of G0.5-OH, G1.5-OH, and G2.5-OH. In addition, a C=O stretching band at 1612 cm^{-1} indicates the formation of a tertiary amide, probably obtained by a reaction of half-generation dendrimers with diethanolamine, which accompanies the weak amide N–H band at 1559 cm^{-1} and the C–N amine stretching of the molecule core at 1117 cm^{-1}.[33]

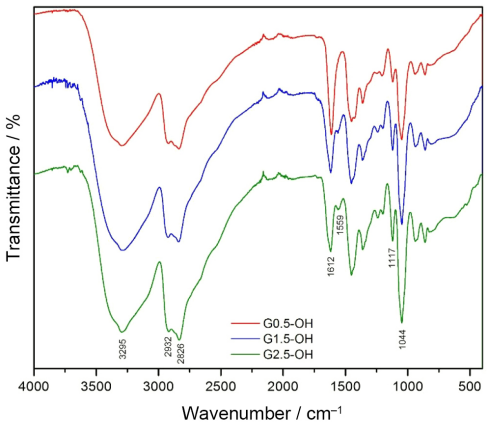

Figure 3. Infrared spectra of PAMAMs with hydroxyl end group.

Figure 4 shows the thermogravimetric analysis curves of the synthesized dendrimers. Mass losses below 140 °C can be attributed to the release of hydration water and organic solvent residues. Dendrimers with ester and amine functional groups degraded above 200 °C (Table 2). According to Table 2, amine-terminal macromolecules are more stable than those containing ester terminals, indicating that the latter requires less energy for degradation. Ester-terminated dendrimers (G0.5, G1.5, and G2.5) had similar onset temperatures (close to 213 °C), while those terminated in amine (G1 and G2) had onset temperature of 227 °C. Meanwhile, hydroxyl-terminal dendrimers degraded near 147 °C (Table 2), indicating lower thermal stability than the other polymers. All PAMAMs fully degraded up to 450 °C except G0.5, whose degradation ended at 250 °C, probably because it is the smallest polymeric molecule.

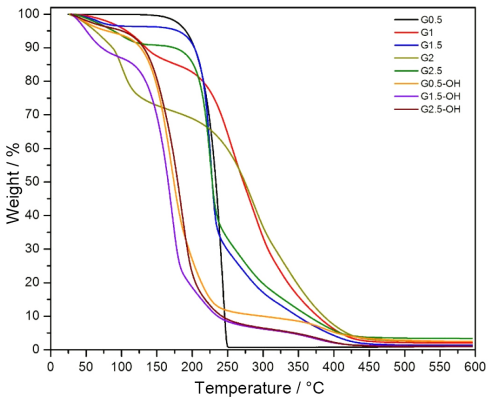

Figure 4. PAMAM thermogravimetric analysis curves.

Table 2. Thermal degradation onset (T_{onset}) and glass transition (T_g) temperature

Sample	T_{onset} / °C		T_g / °C	
	This work	Literature	This work	Literature
G0.5	215		–76	–83[29]
G1	225	184-200[34]	–34	–34[39]
G1.5	213	250[35]	–57	–53[29]
		213[36]		–33[39]
G2	228	200[37]	–47	–3[29]
				0[40]
G2.5	211	–	–77	–44[41]
G0.5-OH	144	150[38]	–75	–
G1.5-OH	147		–79	–
G2.5-OH	150		–82	–

According to Hassan,[34] Deutsch *et al.*[38] and Brabander-van den Berg and Meijer,[42] dendrimers thermally

degrade in a reverse Michael addition reaction (retro-Michael), indicating that these macromolecules undergo end-to-core degradation.

Figure 1 illustrates the reverse reactions of each molecule formed. Thus, it is possible to speculate that the first groups leave the half-generation dendrimers (G0.5, G1.5, and G2.5) according to the structure represented in Figure 5a, while for full-generation PAMAMs (G1 and G2), the leaving group is represented in Figure 5b, and the leaving group of the hydroxyl-terminated ones (G0.5-OH, G1.5-OH and G2.5-OH) is represented in Figure 5c.

The leaving group in Figure 5c has comparatively higher free electron density, it contains two oxygen atoms, one nitrogen atom and five free electron pairs, which favors chemical bond breaking at its junction with the molecule. Therefore, hydroxyl-terminated molecules undergo thermal degradation at lower temperatures, giving them less thermal stability.

The leaving group in Figure 5a has lower free electron density than the previous one, it has only two oxygen atoms and four free electron pairs, which allows us to assume that ester-terminated molecules have greater thermal stability than hydroxyl-terminated ones. On the other hand, Figure 5b represents the lowest free electron density structure, with two nitrogen atoms and two free electron pairs, and therefore amine-terminated molecules are comparatively the most thermally stable. Thus, the thermal stability of the PAMAMs in order is amine-terminal > ester-terminal > hydroxyl-terminal.

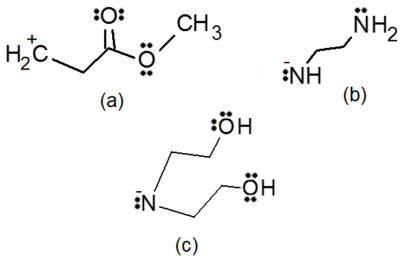

Figure 5. Leaving groups from PAMAM thermal decomposition: (a) ester end group (G0.5, G1.5, and G2.5), (b) amine end group (G1 and G2), and (c) hydroxyl end group (G0.5-OH, G1.5-OH, and G2.5-OH).

The glass transition temperatures (T_g) of G0.5, G1.0, and G1.5 dendrimers were similar to those reported in the literature[29,39] (Table 2). On the other hand, G2.0 and G2.5 samples had lower glass transition temperatures than expected[29,40,41] (Table 2) which allows us to suggest that macromolecules have reduced crosslinking and less intertwining, allowing an easier phase transition. The hydroxyl groups added to G1.5 dendrimers reduced their T_g values, indicating a less energetic phase transition.

CO_2 capture tests and isotherm analysis

The temperature range determination of CO_2 capture for hydroxyl, amine and ester-terminated dendrimers was carried out using a CO_2/N_2 gas stream with 45% v/v CO_2 and temperature from approximately 25 to 120 °C (Figure 6). Experiments showed that only hydroxyl-terminated PAMAM polymers were able to gain mass and, therefore, capture CO_2 from room temperature up to approximately 90 °C. Therefore, gas capture tests were carried out at 40, 60, 80, and 90 °C.

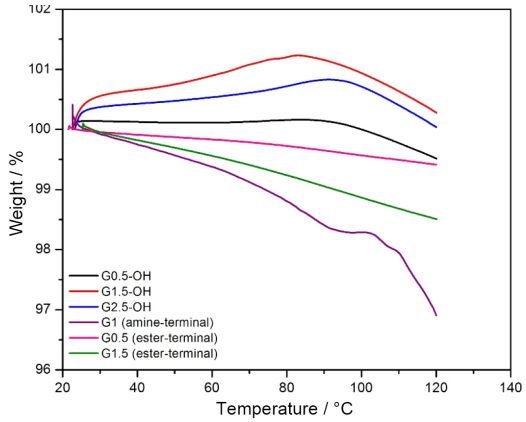

Figure 6. CO_2 capture on PAMAMs containing hydroxyl, amine and ester-terminal functional groups.

Figure 6 shows there was no substantial mass gain by the amine-terminated dendrimer samples. However, Qi *et al.*,[43] Afkhamipour *et al.*,[44] Oh *et al.*,[45] Dashti *et al.*,[46] Strojny *et al.*,[47] and Gutierrez *et al.*[48] all reported the CO_2 capture in aqueous amine solutions, operating in an absorption column with countercurrent flow. These authors emphasized that countercurrent operation favors contact between the gaseous and liquid phases, improving CO_2 capture efficiency. Gautam and Mondal,[49] Liang *et al.*,[50] Fu *et al.*,[51] and Gómez-Díaz *et al.*[52] also highlighted this better contact between phases when gas is bubbled into amine solutions.

The technique used in our research consists of applying a tangential contact between gas phase and the liquid phase surface within a thermogravimetric analysis device, where contact between CO_2-dendrimer occurred only superficially. Therefore, in the case of amine-terminated samples, we suggest that CO_2 capture be carried out using techniques where phases come into bulk contact in the countercurrent flow.

Figures 7, 8, and 9 show the CO_2 solubilization isotherms for G0.5-OH, G1.5-OH, and G2.5-OH PAMAMs. The 40 °C isotherm reached saturation in the partial pressures range used, indicating that solubility equilibrium was

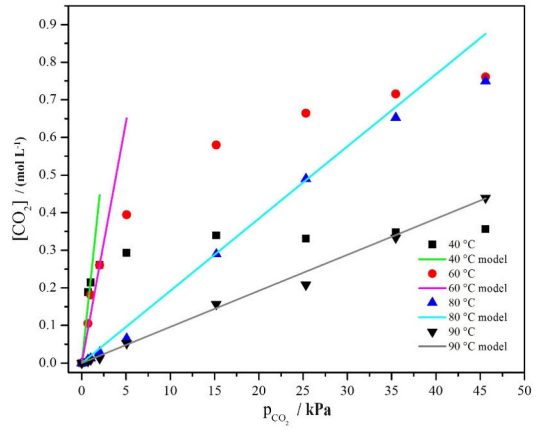

Figure 7. CO_2 capture isotherms for G0.5-OH PAMAM at 40, 60, 80, and 90 °C with fit for Henry's model.

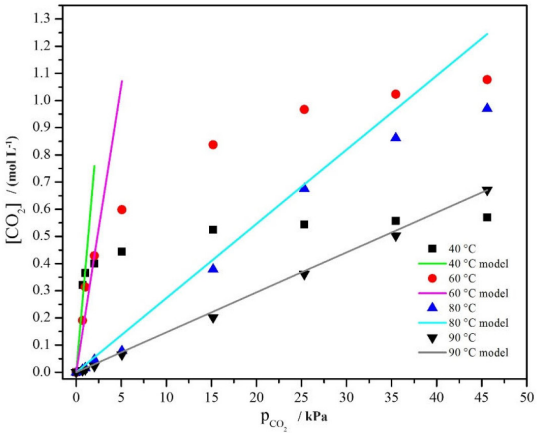

Figure 8. CO_2 capture isotherms for G1.5-OH PAMAM at 40, 60, 80, and 90 °C with fit for Henry's model.

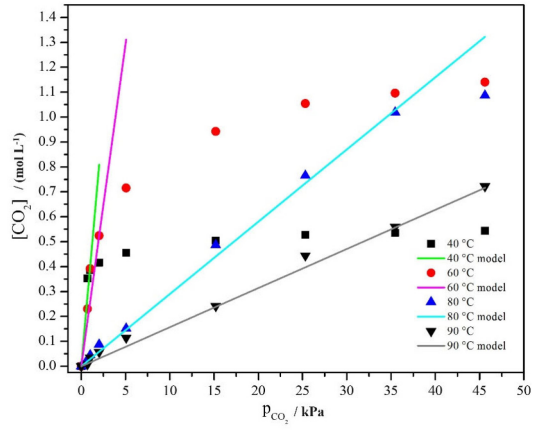

Figure 9. CO_2 capture isotherms for G2.5-OH PAMAM at 40, 60, 80, and 90 °C with fit for Henry's model.

reached. Therefore, for the partial pressures employed, the solution CO_2 + PAMAM could be considered diluted and system molecules were distinguishable in relation to their interaction magnitude. At 40 and 60 °C, the solutions were diluted enough to be considered ideal only at partial pressures below 2 and 5 kPa, respectively. As a result, Henry's model is only appropriate to up to 40 and 60°C isotherms at lower pressures.

The 60, 80, and 90 °C isotherms did not reach saturation until 45 kPa, and so a higher amount of CO_2 could be captured by solubilization. Figures 7, 8, and 9 show that Henry's model adequately fitted both the 80 and 90 °C isotherms up to 45 kPa. This indicates that system constituent molecules were indistinguishable in this high-temperature range. Even when working with higher CO_2 partial pressures, the system could be considered ideal.

At low pressures, CO_2 behaved like an ideal gas, so and, therefore, Henry's model satisfactorily described this research data, making it possible to estimate the solubility constant of the gas. At higher pressures, CO_2 did not behave like an ideal gas, so and in this case we suggest using a more sophisticated model to predict the solubility of real gases in liquid media. Such modeling would require a more complex and in-depth thermodynamic study, which was outside the scope of this study.

During gas capture analysis using hydroxylated dendrimers (G0.5-OH, G1.5-OH and G2.5-OH), we observed that CO_2 solubility in the liquid phase increased with decreasing temperature at low CO_2 partial pressures (< 2 kPa), where Henry's model fitted the experimental data in all isotherms (Table 3). For partial pressures above 2 kPa, the 40 and 60 °C isotherms did not behave as ideal solutions and did not fit Henry's equation. However, above 2 kPa, gas solubilization was maximum at 60 °C, reaching values close to 0.77, 1.08 and 1.14 mol L^{-1} for G0.5-OH, G1.5-OH and G2.5-OH, respectively.

The CO_2 and hydroxylated dendrimer molecules may have interacted through hydrogen bonds, as demonstrated in the Figure 10. Therefore, at high pressures (above 2 kPa) and low temperatures (40 and 60 °C), CO_2 solubilization in dendrimers was enhanced, and CO_2-dendrimer molecular interactions were stronger enough to trap the gas phase. On the other hand, increasing the temperature from 60 to 90 °C weakened the CO_2-dendrimer molecular interactions

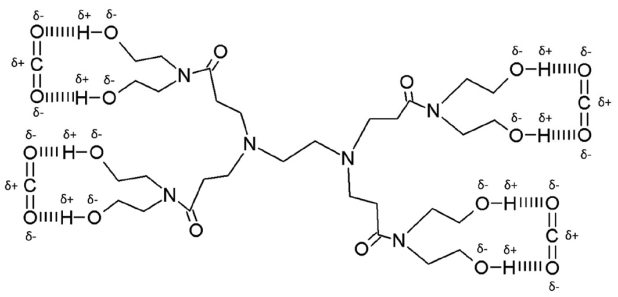

Figure 10. Representative scheme of the interaction mechanism between hydroxyl-terminated dendrimers (G0.5-OH, G1.5-OH, and G2.5-OH) and CO_2.

Table 3. Henry's solubility constant (K_H) for CO_2 solubility in the hydroxyl-terminated dendrimers in different absorption temperatures

T / °C	G0.5-OH		G1.5-OH		G2.5-OH	
	K_H / (mol m^{-3} kPa^{-1})	R^2	K_H / (mol m^{-3} kPa^{-1})	R^2	K_H / (mol m^{-3} kPa^{-1})	R^2
90	9.6	0.992	14.7	0.998	15.7	0.995
80	19.2	0.999	27.3	0.993	29.0	0.999
60	128.4	0.952	211.4	0.935	258.6	0.927
40	220.0	0.961	374.2	0.960	398.4	0.945

T: temperature; K_H: Henry's solubility constant; R^2: correlation coefficient.

and decreased CO_2 solubilization in the liquid phase, i.e., the gas-phase trap became poorer.

The K_H value represents the CO_2 solubility in the absorbent (Table 3). Reducing the temperature increases CO_2 solubility in the absorbent,[25,44,45,49,50,53-59] indicating that intermolecular interactions between the dendrimer and CO_2 molecules are enhanced. In addition, solubility increases for larger dendrimer structures, i.e., G2.5-OH > G1.5-OH > G0.5-OH. We found no similar data on CO_2 solubility in the synthesized dendrimers in the literature for comparison with our calculated data.

Table 4 shows the CO_2 molar concentration for the three samples at four different capture temperatures and 45 kPa CO_2 pressure. The standard deviation was calculated by performing replicates of the central point. CO_2 capture at 40 °C was lower for G0.5-OH and similar for G1.5-OH and G2.5-OH dendrimers. This behavior allows us to speculate that system kinetic energy level at 40 °C is not high enough to promote dendron opening in the G1.5-OH and G2.5-OH samples. Therefore, steric hindrance may have diminished CO_2 penetration in G1.5-OH and G2.5-OH bulk-phase, and solubility did not vary considerably. At 60, 80, and 90 °C, the CO_2 concentration increased with dendrimer structure growth, indicating that gas capture is enhanced in absorbents whose molecules have large numbers hydroxyl groups (see Figure 1).

Table 4. CO_2 concentration (mol L^{-1}) in hydroxylated dendrimers at CO_2 partial pressure of 45 kPa (standard deviation of ± 0.01 mol L^{-1})

Sample	CO_2 concentration / (mol L^{-1})			
Temperature / °C	40	60	80	90
G0.5-OH	0.36	0.77	0.74	0.44
G1.5-OH	0.56	1.08	0.97	0.67
G2.5-OH	0.54	1.14	1.09	0.72

The solubility of CO_2 achieved by hydroxylated dendrimers (Table 4) had values consistent with studies presented in the literature. In this regard, Qi *et al.*[43] carried out CO_2 capture tests in an absorption tower, using aqueous amine solutions. The absorbent solutions achieved a solubility range of 0.71-1.09 mol L^{-1} at 40 °C and atmospheric pressure. Using amine solutions in a bubble column reactor, Gautam and Mondal[49] also obtained a CO_2 solubility range between 0.65 and 1.09 mol L^{-1}. In this case, the system was operated at atmospheric pressure and temperatures ranging between 25 and 60 °C.

Despite not achieving the best operational design, this study revealed good CO_2 absorption yields. Therefore, we can suggest that the application of the hydroxylated dendrimers demonstrated here in a system operating in countercurrent or in a bubble column reactor can achieve even better solubility results, since more efficient contact between the gas and liquid phases will be possible.

Table 5 presents the thermodynamic state functions calculated for the CO_2 solubilization in the PAMAM hydroxylated generations. For all generations (G0.5-OH, G1.5-OH, and G2.5-OH), CO_2 solubilization was a spontaneous process ($\Delta G < 0$), and the lower the temperature, the more spontaneous it was. For a given constant temperature, greater the dendrimer generation was associated with more spontaneous CO_2 capture. Furthermore, gas solubilization enthalpy was exothermic ($\Delta H < 0$) indicating strong CO_2-dendrimer molecular interactions and large heat release during CO_2 capture. An exothermic process was also found by Liang *et al.*[50] and Sadegh *et al.*,[60] where aqueous amine solutions interacted with CO_2 and assumed solubilization enthalpy values similar (–66.9 and –54.6 kJ mol^{-1}) to those reported in Table 5.

Absorptions with hydroxylated dendrimers present negative entropy variation, indicating a decrease in the solute degrees of freedom during gas-liquid solubilization. That is, CO_2 gas molecules migrated from a stage of greater movement freedom to a more ordered stage in the absorbent bulk, so $\Delta S < 0$.[61-63] Furthermore, this decrease in solute degrees of freedom was approximately the same for all dendrimer generations, indicating that the solubilization process is similar at the molecular level in these materials. Li *et al.*[26] and Kurnia *et al.*[27] also reported that negative entropy might indicate higher molecular ordering degree when CO_2 is solubilized in PAMAM. Global entropy might always be positive, and it is given by the sum of

Table 5. Thermodynamic properties of CO_2 solubilization for the hydroxyl-terminated dendrimers (reference: T = 25 °C and $K^* = 0.34$ mol m^{-3} kPa^{-1})

T / °C	G0.5-OH			G1.5-OH			G2.5-OH		
	ΔG_{sol} / (kJ mol^{-1})	ΔH_{sol} / (kJ mol^{-1})	ΔS_{sol} / (kJ mol^{-1} K^{-1})	ΔG_{sol} / (kJ mol^{-1})	ΔH_{sol} / (kJ mol^{-1})	ΔS_{sol} / (kJ mol^{-1} K^{-1})	ΔG_{sol} / (kJ mol^{-1})	ΔH_{sol} / (kJ mol^{-1})	ΔS_{sol} / (kJ mol^{-1} K^{-1})
90	–10.08	–61.43	–0.14	–11.37	–64.24	–0.14	–11.57	–64.78	–0.15
80	–11.84			–12.87			–13.05		
60	–16.43			–17.81			–18.37		
40	–16.84			–18.23			–18.39		

T: temperature; K*: Henry solubility constant of CO_2 in water at 298 K; ΔG_{sol}: Gibbs' energy; ΔH_{sol}: enthalpy of the solution; ΔS_{sol}: entropy.

neighborhood entropy (ΔS_N) with process entropy, i.e., ΔS_{sol}. Thus, ΔS_N can be positive and greater than ΔS_{sol} in modulus during the solubilization process.

At low pressures, CO_2 behaves like an ideal gas, and, therefore, Henry's model satisfactorily described these research data, enabling us to estimate the solubility constant K_H of the gas. At higher pressures, CO_2 did not behave like an ideal gas, and in this case we suggest using a more sophisticated model to predict the solubility of real gases in liquid media. Such modeling would require a more complex and in-depth thermodynamic study, which was not in the scope of this work.

Conclusions

Thermogravimetric analysis revealed that CO_2 capture by gas absorption in the liquid dendrimer occurred, since mass incorporation was verified in an adequate temperature range. Mass gain occurred only in hydroxyl-terminated molecules, while amine and ester-terminated molecules were unable to absorb CO_2. The amine-terminated dendrimers were unable to capture CO_2, probably because the operational design used did not help to by promoting good contact between the gas and liquid phases. However, the proposed absorbent system allowed hydroxyl-terminated dendrimers to exhibit good CO_2 absorption results. The highest CO_2 absorption capacity was achieved by the dendrimer with the highest number of hydroxyls (G2.5-OH) at a temperature of 60 °C (1.14 mol L^{-1}). Henry's model adequately fitted all absorption isotherms only at partial pressures lower than 2 kPa. However, this model was adequate up to 45 kPa for 80 and 90 °C isotherms. Therefore, the CO_2-PAMAM solution can only be considered ideal in specific CO_2 partial pressure ranges. CO_2-dendrimer molecular interactions were influenced by the absorption temperature, and interactions were stronger at 60 °C, indicated by greater solubilization. The calculated thermodynamic properties indicated that solubilization is a spontaneous and exothermic process. Based on the results achieved in this work, the thermal degradation temperatures were similar for dendrimers with the same terminal functional group, and thermal stability of hydroxyl-terminated molecules was lower compared with amine and ester-terminated molecules. This was related to the higher free electron density of the leaving group, favoring breakage of the chemical bond at its junction with the molecule. Thermal analysis also suggested that lower glass transition temperatures (T_g) are related to molecules with reduced crosslinking and less intertwining, allowing easier phase transition.

Acknowledgments

We thank the Fundação Carlos Chagas Filho de Amparo à Pesquisa do Estado do Rio de Janeiro (FAPERJ) for research grants (E-26/010000982/2019, E-26/200.016/2020 (252750) E-26/200.974/2021); Conselho Nacional de Desenvolvimento Científico e Tecnológico (CNPq) for financial support (grant 305.565/2022-2); and the Laboratório de Tecnologias do Hidrogênio (LabTech/EQ/UFRJ) for supporting the CO_2 capture analyses.

Author Contributions

Thiago M. Rossi was responsible for the formal analysis, investigation, methodology, writing original draft; Monique L. Almeida for the formal analysis and investigation; Mariana M. V. M. Souza for the conceptualization, investigation, methodology; Elizabete F. Lucas for the conceptualization, data curation, funding acquisition, project administration, resources, supervision, writing review and editing; Bluma G. Soares for the resources, funding acquisition, project administration, supervision, writing review and editing.

References

1. Climate.gov, *Atmospheric Carbon Dioxide*, https://www.climate.gov/news-features/understanding-climate/climate-change-atmospheric-carbon-dioxide, accessed in May 2024.
2. International Energy Agency (IEA), *Greenhouse Gas Emissions from Energy Data Explorer*, https://www.iea.org/data-and-statistics/data-tools/greenhouse-gas-emissions-from-energy-data-explorer, accessed in May 2024.

3. Observatório do Clima, *Brazil Should Cut Emissions by 81% by 2030*, https://www.oc.eco.br/en/brazil-cut-emissions-81-2030-oc-says/, accessed in May 2024.
4. International Energy Agency (IEA), *Global Energy Review: CO_2 Emissions in 2021*, https://www.iea.org/reports/global-energy-review-co2-emissions-in-2021-2, accessed in May 2024.
5. Observatório do Clima, *21 Recados Fundamentais do Novo Relatório do IPCC*, https://www.oc.eco.br/21-recados-fundamentais-do-novo-relatorio-do-ipcc/, accessed in May 2024.
6. Reddy, M. K. R.; Xu, Z. P.; da Costa, J. C. D.; *Ind. Eng. Chem. Res.* **2008**, *47*, 2630. [Crossref]
7. Odunlami, O. A.; Vershima, D. A.; Oladimeji, T. E.; Nkongho, S.; Ogunlade, S. K.; Fakinle, B. S.; *Results Eng.* **2022**, *15*, 100512. [Crossref]
8. Meng, F.; Meng, Y.; Ju, T.; Han, S.; Lin, L.; Jiang, J.; *Renewable Sustainable Energy Rev.* **2022**, *168*, 112902. [Crossref]
9. Aghel, B.; Janati, S.; Wongwises, S.; Shadloo, M. S.; *Int. J. Greenhouse Gas Control* **2022**, *119*, 103715. [Crossref]
10. Li, J.; Liang, H.; Liu, J.; Wang, Z.; *Int. J. Pharm.* **2018**, *546*, 215. [Crossref]
11. Kovvali, A. S.; Chen, H.; Sirkar, K. K.; *J. Am. Chem. Soc.* **2000**, *122*, 7594. [Crossref]
12. Kovvali, A. S.; Sirkar, K. K.; *Ind. Eng. Chem. Res.* **2001**, *40*, 2502. [Crossref]
13. Duan, S.; Kouketsu, T.; Kazama, S.; Yamada, K.; *J. Membr. Sci.* **2006**, *283*, 2. [Crossref]
14. Kai, T.; Taniguchi, I.; Duan, S.; Chowdhury, F. A.; Saito, T.; Yamazaki, K.; Ikeda, K.; Ohara, T.; Asano, S.; Kazama, S.; *Energy Procedia* **2013**, *37*, 961. [Crossref]
15. Duan, S.; Kai, T.; Saito, T.; Yamazaki, K.; Ikeda, K.; *Membranes* **2014**, *4*, 200. [Crossref]
16. Chau, J.; Jie, X.; Sirkar, K. K.; *Chem. Eng. J.* **2016**, *305*, 212. [Crossref]
17. Borgohain, R.; Mandal, B.; *J. Membr. Sci.* **2020**, *608*, 118214. [Crossref]
18. Fadhel, B.; Hearn, M.; Chaffee, A.; *Microporous Mesoporous Mater.* **2009**, *123*, 140. [Crossref]
19. Shah, K. J.; Imae, T.; Shukla, A.; *RSC Adv.* **2015**, *5*, 35985. [Crossref]
20. Tomalia, D. A.; Baker, H.; Dewald, J.; Hall, M.; Kallos, G.; Martin, S.; Roeck, J.; Ryder, J.; Smith, P.; *Polym. J.* **1985**, *17*, 117. [Crossref]
21. Froimowicz, P.; Gandini, A.; Strumia, M.; *Tetrahedron Lett.* **2005**, *46*, 2653. [Crossref]
22. Barros, H. N. S.; Weisblum, M. A.; Martins, M. F.; Bertolino, L. C.; da Silva, I. G. M.; Rossi, T. M.; Soares, B. G.; Lucas, E. F.; *Pet. Sci. Technol.* **2023**, *1*, 1. [Crossref]
23. Alves, B. F.; Rossi, T. M.; Marques, L. C. C.; Soares, B. G.; Lucas, E. F.; *Fuel* **2023**, *332*, 125962. [Crossref]
24. Atkins, P.; de Paula, J.; *Físico-Química*, vol. 1, 9th ed.; Livros Técnicos e Científicos: Rio de Janeiro, 2015.
25. Gonzalez-Miquel, M.; Bedia, J.; Abrusci, C.; Palomar, J.; Rodriguez, F.; *J. Phys. Chem. B* **2013**, *117*, 3398. [Crossref]
26. Li, X.; Hou, M.; Zhang, Z.; Han, B.; Yang, G.; Wanga, X.; Zou, L.; *Green Chem.* **2008**, *10*, 879. [Crossref]
27. Kurnia, K. A.; Harris, F.; Wilfred, C. D.; Abdul Mutalib, M. I.; Murugesan, T.; *J. Chem. Thermodyn.* **2009**, *41*, 1069. [Crossref]
28. Kannaiyan, D.; Imae, T.; *Langmuir* **2009**, *25*, 5282. [Crossref]
29. Niu, Y.; Lu, H.; Wang, D.; Yue, Y.; Feng, S.; *J. Organomet. Chem.* **2011**, *696*, 544. [Crossref]
30. Şenel, M.; Çevik, E.; *Curr. Appl. Phys.* **2012**, *12*, 1158. [Crossref]
31. Şenel, M.; Nergiz, C.; Çevik, E.; *Sens. Actuators, B* **2013**, *176*, 299. [Crossref]
32. Cao, D.; Qin, L.; Huang, H.; Feng, M.; Pan, S.; Chen, J.; *Mol. BioSyst.* **2013**, *9*, 3175. [Crossref]
33. Silverstein, R. M.; Webster, F. X.; Kiemle, D. J.; *Spectrometric Identification of Organic Compounds*, vol. 1, 7th ed.; John Wiley & Sons: New York, 2005.
34. Hassan, M. L.; *J. Appl. Polym. Sci.* **2006**, *101*, 2079. [Crossref]
35. Huang, J. F.; Luo, H.; Liang, C.; Sun, I. W.; Baker, G. A.; Dai, S.; *J. Am. Chem. Soc.* **2005**, *127*, 12784. [Crossref]
36. Ilaiyaraja, P.; Deb, A. K. S.; Sivasubramanian, K.; Ponraju, D.; Venkatraman, B.; *J. Hazard. Mater.* **2013**, *250*, 155. [Crossref]
37. Kirbay, F. O.; Yalcinkaya, E. E.; Atik, G.; Evren, G.; Unal, B.; Demirkol, D. O.; Timur, S.; *Biosens. Bioelectron.* **2018**, *109*, 286. [Crossref]
38. Deutsch, D. S.; Siani, A.; Fanson, P. T.; Hirata, H.; Matsumoto, S.; Williams, C. T.; Amiridis, M. D.; *J. Phys. Chem. C* **2007**, *111*, 4246. [Crossref]
39. Mijović, J.; Ristić, S.; Kenny, J.; *Macromol.* **2007**, *40*, 5212. [Crossref]
40. Dvornic, P. R.; Hartmann-Thompson, C.; Keinath, S. E.; Hill, E. J.; *Macromol.* **2004**, *37*, 7818. [Crossref]
41. Borowska, K.; Laskowska, B.; Magoń, A.; Mysliwiec, B.; Pyda, M.; Wołowiec, S.; *Int. J. Pharm.* **2010**, *398*, 185. [Crossref]
42. Brabander-van den Berg, E. M. M.; Meijer, E. W.; *Angew. Chem., Int. Ed.* **1993**, *32*, 1308. [Crossref]
43. Qi, Z.; Liu, F.; Ding, H.; Fang, M.; *Fuel* **2023**, *350*, 128726. [Crossref]
44. Afkhamipour, M.; Seifi, E.; Esmaeili, A.; Shamsi, M.; Borhani, T. N.; *Fuel* **2024**, *356*, 129607. [Crossref]
45. Oh, H. T.; Lee, J. C.; Lee, C. H.; *Fuel* **2022**, *314*, 122768. [Crossref]
46. Dashti, A.; Raji, M.; Alivand, M. S.; Mohammadi, A. H.; *Fuel* **2020**, *264*, 116616. [Crossref]
47. Strojny, M.; Gładysz, P.; Hanak, D. P.; Nowak, W.; *Energy* **2023**, *284*, 128599. [Crossref]
48. Gutierrez, J. P.; Tarifa, E. E.; Erdmann, E.; *Energy* **2018**, *159*, 1016. [Crossref]
49. Gautam, A.; Mondal, M. K.; *Fuel* **2023**, *331*, 125864. [Crossref]

50. Liang, Y.; Liu, H.; Rongwong, W.; Liang, Z.; Idem, R.; Tontiwachwuthikul, P.; *Fuel* **2015**, *144*, 121. [Crossref]
51. Fu, D.; Zhang, P.; Mi, C.; *Energy* **2016**, *101*, 288. [Crossref]
52. Gómez-Díaz, D.; Grueiro, J.; Navaza, J. M.; Noval, C.; *Energy* **2018**, *153*, 568. [Crossref]
53. Xiao, M.; Liu, H.; Gao, H.; Liang, Z.; *J. Chem. Thermodyn.* **2018**, *122*, 170. [Crossref]
54. Pandey, D.; Mondal, M. K.; *Chem. Eng. J.* **2021**, *410*, 128334. [Crossref]
55. Oliveira, L. M. S. L.; Nunes, R. C. P.; Ribeiro, Y. L. L.; Coutinho, D. M.; Azevedo, D. A.; Dias, J. C. M.; Lucas, L. F.; *J. Braz. Chem. Soc.* **2018**, *29*, 2158. [Crossref]
56. Valente, A. C. F.; Nunes, R. C. P.; Lucas, E. F.; *J. Braz. Chem. Soc.* **2023**, *34*, 83. [Crossref]
57. Carvalho, S. P.; Dip, R. M. M.; Lucas, E. F.; *J. Braz. Chem. Soc.* **2020**, *31*, 2583. [Crossref]
58. Nunes, R. C. P.; Valle, M. R. T.; Reis, W. R. D.; Aversa, T. M.; Filipakis, S. D.; Lucas, E. F.; *J. Braz. Chem. Soc.* **2019**, *30*, 1241. [Crossref]
59. Fu, K.; Liu, C.; Wang, L.; Huang, X.; Fu, D.; *Energy* **2021**, *220*, 119735. [Crossref]
60. Sadegh, N.; Stenby, E. H.; Thomsen, K.; *Fuel* **2015**, *144*, 295. [Crossref]
61. Ammendola, P.; Raganati, F.; Chirone, R.; *Chem. Eng. J.* **2017**, *322*, 302. [Crossref]
62. Martins, M. F.; Aversa, T. M.; da Silva, C. M. F.; da Silva, E. D.; Lucas, E. F.; *J. Braz. Chem. Soc.* **2023**, *34*, 866. [Crossref]
63. Lordeiro, F. B.; Altoé, R.; Hartmann, D.; Filipe, E. J. M.; González, G.; Lucas, E. F.; *J. Braz. Chem. Soc.* **2021**, *32*, 741. [Crossref]

Submitted: February 26, 2024
Published online: May 22, 2024